Potential of melt pond fraction retrieval from high spatial resolution AMSR-E/2 channels

Tanaka, Y. & Scharien, R. K.

2022

Potential of Melt Pond Fraction Retrieval From High Spatial Resolution AMSR-E/2 Channels

Yasuhiro Tanaka and Randall Kenneth Scharien

***Abstract*— Estimation of melt pond fraction (MPF) using the Advanced Microwave Scanning Radiometer for the Earth Observing System (EOS)/2 (AMSR-E/2) brightness temperature (T_B) data is required for enhancing understanding of the role of melt ponds in the Arctic and in the earth's climate system. An original MPF retrieval is based on gradient ratio (GR), defined as the normalized difference between the 6.9 GHz horizontal (H) channel and the 89.0 GHz vertical channel GR(6/89) of AMSR-E. However, using the coarsest spatial resolution 6.9 GHz channel includes potential land contamination in T_B in regions of narrow waterways such as the Canadian Arctic Archipelago (CAA). This letter aims to provide a higher resolution MPF product, derived by using 10.7, 18.7, 23.8, 36.5, and 89.0 GHz T_Bs at H-polarization instead of the 6.9 GHz T_B H-polarization in the GR calculation. For GR(10/89)- and GR(18/89)-based MPF retrievals, the difference standard deviations were ∼3.8%. This is lower than the ∼14.3% standard deviation of the GR(23/89)-, GR(36/89)-, and PR(89)-based MPF retrievals. Our results suggest that the GR(10/89) and (18/89) MPF retrievals are available at a product quality similar to the original GR(6/89)-based MPF retrieval. We recommend that the GR(18/89) MPF retrieval adopted is used in nearshore environments such as in the CAA.**

***Index Terms*— Advanced microwave scanning radiometer for the Earth Observing System (EOS) (AMSR-E), AMSR2, Canadian Arctic Archipelago (CAA), melt pond fraction (MPF), melt season, passive microwave, sea ice.**

I. Introduction

POOLS of liquid water, called melt ponds, form on the ice during the Arctic summer melt season. A better knowledge of the spatio-temporal evolution of melt pond fraction (MPF), i.e., the percentage of a given area covered with pond water surface, enhances our knowledge of the role of melt ponds in the Arctic and in the earth's climate system. Moreover, sea ice concentration estimates from passive microwave observations, obtained daily over polar regions, can be highly inaccurate during summer melt season due to the expansion of melt ponds [1], [2]. Accurate MPF estimates could play an important role in optimizing the sea ice concentration techniques [1], [2].

An original MPF retrieval from the Advanced Microwave Scanning Radiometer for the Earth Observing System (EOS) (AMSR-E) was developed by Tanaka *et al.* [3] and adopted the spectral gradient ratio (GR), the normalized difference between measured brightness temperatures (T_Bs) from the 6.9 GHz horizontal and 89.0 GHz vertical polarization channels (H-pol and V-pol, respectively) GR(6/89) given below (1). The retrieval was developed using an empirically derived linear regression between GR(6/89) and ship-borne MPF observations in the following equations [3]:

$$\mathrm{GR}(f_1/f_2) = \frac{T_B(f_1) - T_B(f_2)}{T_B(f_1) + T_B(f_2)} \tag{1}$$

$$\mathrm{MPF} = 15.2 - 158.9 \cdot \mathrm{GR}(f_1/f_2) \tag{2}$$

where $f_1 = T_B$ at 6.9 GHz H-pol channel and $f_2 = T_B$ at 89.0 GHz V-pol channel in the original MPF retrieval. The retrieval was evaluated using optical remote sensing data [3], [4], resulting in a difference between MPFs from AMSR-E and optical data of less than 5% on eight-day average basis in most regions [3] and 10% on a day-by-day basis in the Canadian Arctic Archipelago (CAA) [4].

The T_B from the finest spatial resolution (or the smallest footprint) 89.0 GHz channels is affected by atmospheric influence (cloud liquid water and water vapor). In the MPF retrieval from AMSR-E [3], the influences are minimized by implementing two weather filters [5]. In contrast, the T_B from the coarsest spatial resolution (or the largest footprint) 6.9 GHz channels is minimally affected by the atmosphere. However, using the 6.9 GHz frequency in regions characterized by narrow channels such as CAA leads to land contamination in measured T_Bs. Since the footprint size decreases with increasing frequency, using 10.7, 18.7, 23.8, 36.5, and 89.0 GHz instead of 6.9 GHz channels in the GR of (1) will decrease the effect of land contamination on T_Bs (and MPF). Moreover, next to around 6 GHz frequency these higher frequencies (particularly H-pol) are sensitive to surface liquid water [6].

In this letter, we examine the potential for MPF retrieval using these higher frequency (or smaller footprint) channels instead of 6.9 GHz in a manner similar to the original GR(6/89) method. Regression coefficients for MPF retrieval are presented for modified GRs and compared to the original GR(6/89) one. This letter is organized as follows: In Section II, data products used in this letter are summarized, and in Section III the original MPF retrieval method and analysis used here are described. Sections IV and V present the results and discussion, and the conclusion obtained from our analysis, respectively. The findings of this letter are expected to enable the selection of an MPF retrieval method that is similar to the original one, with the land contamination effect minimized.

Manuscript received September 15, 2020; revised October 14, 2020; accepted November 1, 2020. Date of publication December 7, 2020; date of current version December 15, 2021. *(Corresponding author: Yasuhiro Tanaka.)*

Yasuhiro Tanaka is with the Earth Observation Research Center (EORC), Japan Aerospace Exploration Agency (JAXA), Tsukuba 305-8505, Japan (e-mail: tanaka.yasuhiro@jaxa.jp).

Randall Kenneth Scharien is with the Department of Geography, University of Victoria, Victoria, BC V8P 3C2, Canada (e-mail: randy@uvic.ca).

Digital Object Identifier 10.1109/LGRS.2020.3038888

TABLE I
SUMMARY OF THE FOUR DATA PRODUCTS USED IN THIS STUDY

Data Product	Parameters [Unit]	Channels used (footprint size in km)	Period used (Provision period)
Canadian Ice Service Arctic Regional Sea Ice Charts in SIGRID-3 Format, Version 1	Sea ice concentration [tenths]	–	2006–2018 (2006–present)
Aqua AMSR-E Level-1R	Brightness temperature [K]	6H (43 × 75), 10H (29 × 51), 18H (16 × 27), 23H (18 × 32), 36H (8 × 14), 89HV (4 × 6)	2006–2011 (2002–2011)
GCOM-W1 AMSR2 Level-1R	Brightness temperature [K]	6H (35 × 62), 10H (24 × 42), 18H (14 × 22), 23H (15 × 26), 36H (7 × 12), 89HV (3 × 5)	2012–2018 (2012–present)
DMSP SSM/I-SSMIS Daily Polar Gridded Brightness Temperatures, Version 5	Brightness temperature [K]	19V (45 × 70), 37V (30 × 38)	2006–2018 (1987–present)

II. DATA

Table I shows a summary of the four data products used in this study. We used the Canada Ice Service (CIS) weekly ice charts in Sea Ice Geo-Referenced Information and Data (SIGRID)-3 format [7], gridded on a 25 km polar stereographic projection grid. The totally ice-covered areas (10/10 sea ice concentration) within the landfast ice area of the CAA were examined. This ensured no open water contamination in the AMSR-E/2 MPF retrievals, for example, prior to the breakup of the landfast ice in late summer.

We used the AMSR-E and AMSR2 Level-1R (L1R) T_B swath products [8] for estimating melt onset (MO) and MPF. The L1R products provide single swath T_Bs at 6.9, 7.3 (AMSR2 only), 10.7, 18.7, 23.8, 36.5, and 89.0 GHz. All frequencies have H-pol and V-pol channels. The footprint size differs substantially for each frequency, with higher frequencies having smaller footprint sizes (Table I) since the AMSR2 was designed with a sharp antenna beam for each frequency. The L1R product modified by an antenna pattern matching technique is made to match the T_B of homogeneous footprint size of lower frequencies [8]. In this study, we used the T_Bs from channels shown in Table I, matching to the largest footprint (highest frequency) in each GR (f_{target}, see Fig. 1). The T_Bs at all frequencies are resampled as ascending and descending average values on 25 km stereographic projection grid to have a one-to-one comparison with the GR(6/89) MPF. To avoid the land contamination when resampling the 25 km grid, the T_Bs with the ratio of land surface below 1% (sea surface above 99%) in the footprint from the land sea flag data is used.

III. METHODOLOGY

Fig. 1 shows a flowchart to obtain potential GR- and polarization ratio (PR)-based MPFs, and original GR-based MPF. The AMSR-E/2 frequencies are insensitive to water salinity and cannot distinguish between saline seawater (open water) and freshwater (pond water) in cold water areas [6]. Moreover, in the freeze-up period (outside melt season), microwave radiation emitted from sea ice is affected by ice volume scattering originating within the ice, and also from the overlying snow. Therefore, results from our analysis are constrained by the following two conditions.

1) We used grid cell data corresponding to totally ice-covered areas taken as 10/10 sea ice concentration from CIS ice charts, to avoid the open water contamination in the AMSR-E/2 MPF retrievals.
2) We used grid cell data from the period between MO and freeze onset (FO) dates only. MO and FO date detections are based on the dynamic threshold variability technique using time series T_B with V-pol at 36.5 GHz channel from the input AMSR-E/2 L1R product [9] and the T_Bs with V-pol at 19 and 37 GHz [10] from the Defense Meteorological Satellite Program (DMSP) the Special Sensor Microwave/Imager–the Special Sensor Microwave Imager/Sounder (SSM/I-SSMIS) Daily Polar Gridded T_B product [11], respectively. In 2012, the MO detections using [9] are not possible since the AMSR2 data are available from 4 July. MO in 2012 is instead detected using the melt/freeze-up algorithm 10]. In the case where the break-up occurs between MO and FO dates, the grid cell over the range between MO and break-up dates is used. Here, we defined the break-up date when CIS ice concentration dropped below 100%.

As described in Section I, the original MPF retrieval algorithm by Tanaka *et al.* [3] uses a linear regression between GR (6/89) of (1) and ship-borne observations in (2). Using the coarse spatial resolution 6.9 GHz channel in the original MPF algorithm leads to land contamination in the MPF estimated for nearshore areas. We compared other available $f_1 = 10.7$, 18.7, 23.8, or 36.5 GHz H-pol channel and $f_2 = 89.0$ GHz V-pol channel combinations for estimating MPF with the originally used GR(6/89) from [3]. The H-pol channel at 10.7, 18.7, 23.8, and 36.5 GHz is chosen here since the emissivity difference between water and snow/ice is larger for H-pol than V-pol [6]. We also evaluated the PR at 89 GHz for comparison to GR(6/89), using the following equation for PR (89):

$$\text{PR}(89) = \frac{T_B(89V) - T_B(89H)}{T_B(89V) + T_B(89H)} \tag{3}$$

Note that the AMSR2 data are available from July in 2012, which is a loss of approximately half of the melt season for that year. As well, the analysis is limited to ascending average T_B for this letter since it was found to be similar to using the descending average T_B.

For the selection of the potential MPF retrieval method that is similar to the original one, we compared MPFs from the original GR(6/89) to potential GR(f_1/f_2) [also PR(89)].

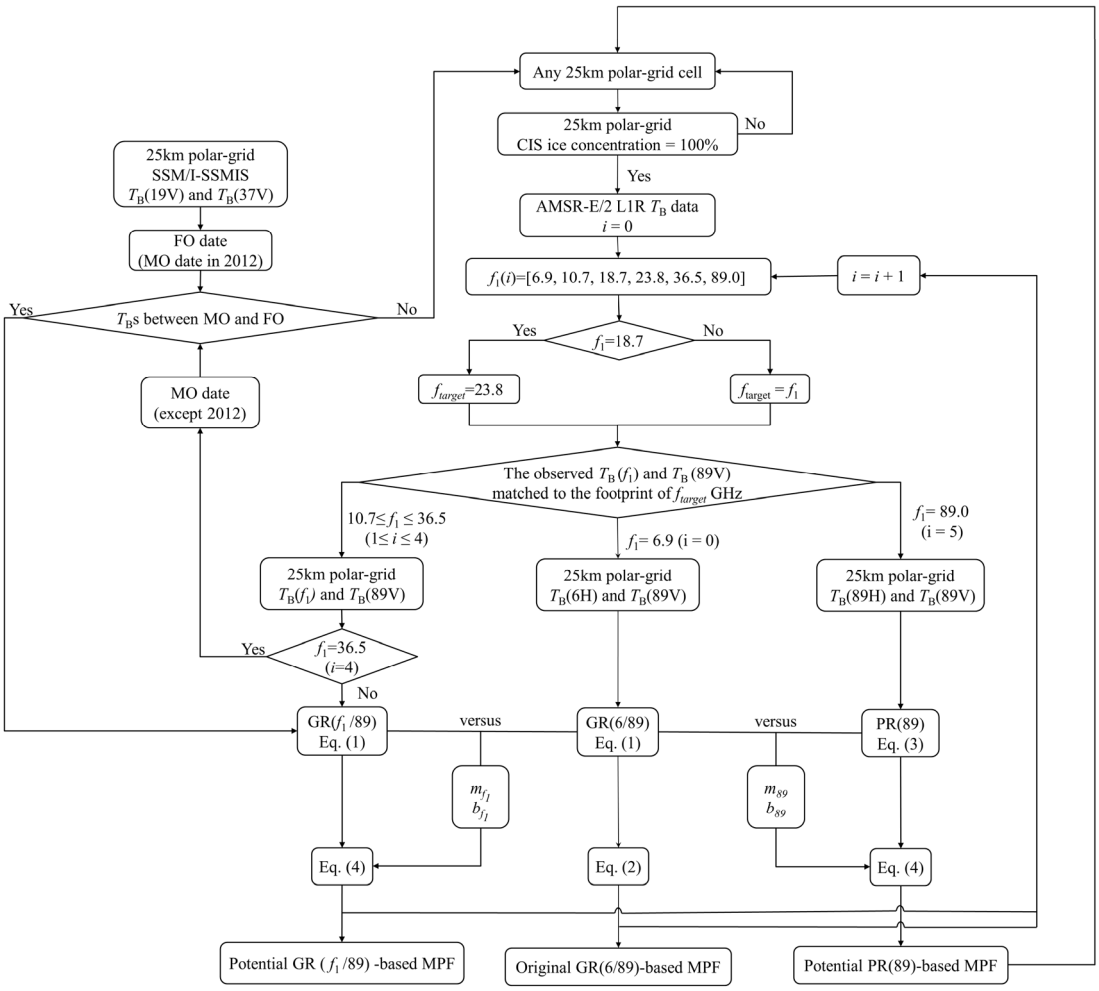

Fig. 1. Flowchart to obtain potential GR- and PR-based MPFs, and original GR-based MPF. See sentence in Sections II and III for more explanation in our analysis conditions.

TABLE II

YEARLY STATISTICS OF DIFFERENCE OF MPFS RETRIEVED FROM ORIGINAL AND POTENTIAL GRS OR PR DURING 2006–2018

Year	Number of grid cell	Difference [%]					Standard deviation [%]				
		GR (10/89)	GR (18/89)	GR (23/89)	GR (36/89)	PR(89)	GR (10/89)	GR (18/89)	GR (23/89)	GR (36/89)	PR(89)
2006	11744	-0.6	-1	-1.7	-1.1	0.8	1.8	3.8	5	7.5	14.3
2007	47697	-0.1	-0.4	-0.7	-1.5	2.7	1.4	3.1	4.6	6.6	11.1
2008	31840	0	-0.2	-0.2	-1.2	2.6	1.5	3.2	4.3	6.5	9.1
2009	41367	0	-0.1	0	-0.4	1.6	1.3	2.7	3.7	5	6.9
2010	31105	0.1	-0.1	-0.2	-1	0.9	1.6	3	3.8	5.2	7.9
2011	39553	0	-0.4	-0.5	-0.8	3.2	1.5	3.6	5.2	7	9.9
2012	7306	-0.1	-1.8	-4.8	-9.3	-22.2	1.4	2.5	3.7	4.3	7.9
2013	46948	-0.1	-0.7	-1.1	-2	2.1	1.1	2.5	3.6	5.3	9.8
2014	43896	0.2	0.1	0	-0.1	2.8	1.3	3.7	5.7	8.4	9.3
2015	36139	0.3	0.2	0.2	-1	2	1.4	3.5	4.9	6.4	8.2
2016	42093	-0.1	-0.4	-0.7	-1	2.8	1.4	3.4	5	7.1	10.7
2017	34765	-0.1	-0.2	0	0.1	2.7	1.3	3.2	4.6	6.9	8.7
2018	42103	0	-0.2	-0.1	0.8	3.5	1.2	3	4.3	6.3	8.4

This result is summarized as average MPF difference (potential GRs- or PR-based MPF minus original GR-based MPF) and its standard deviation during 2006–2018 in the CAA using a 25 km polar grid (see Table II).

IV. RESULTS AND DISCUSSION

To select the potential MPF retrieval that is similar to the original MPF retrieval, the results of GR(6/89) combination were compared with those of other combinations.

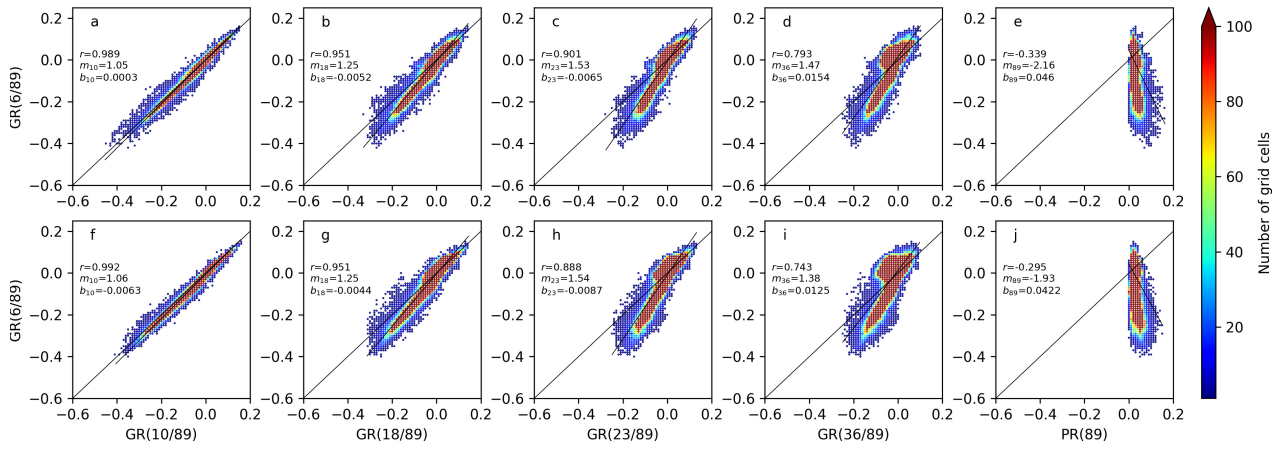

Fig. 2. Relationship between original GR(6/89) and potential GR(10/89), GR(18/89), GR(23/89), GR(36/89), and PR(89) for MPF retrievals using (a)–(e) AMSR-E and (f)–(j) AMSR2 data. r: correlation coefficient, m: slope, b: intercept.

Fig. 2 shows the relationship between original GR(6/89) and potential GR(f_1/f_2) or PR(89), along with regression coefficients slope (m) and intercept (b), and the correlation coefficient (r). The highest correlations ($r > 0.99$) and slopes of the linear regression closest to one were obtained for GR(10/89) from AMSR-E and AMSR2 [Fig. 2(a) and (f)]. For other potential GR combinations, the correlations and slopes decreased and became steeper, respectively, in order of GR(10/89), GR(18/89), GR(23/89), GR(36/89), and PR(89) [Fig. 2(b)–(e) and (g)–(j)]. Moreover, the dynamical range of potential GR values became narrower with increasing frequency of the f_1. This demonstrates that GR combination using higher frequency channels are potentially less sensitive to changes in MPF.

The original MPF retrieval depends on the empirical regression coefficients for the relationship between GR(6/89) and ship-borne measurements of MPF. Here, we corrected the potential GR(10/89), GR(18/89), GR(23/89), GR(36/89), and PR(89) values to the original GR(6/89) values using the regression coefficients for AMSR-E/2 data obtained in Fig. 2. To obtain the original MPFs from the corrected GRs, we produced the following correction formula:

$$\mathrm{MPF} = 15.2 - 158.9 \cdot \begin{cases} m_{f_1}\ \mathrm{GR}(f_1/f_2) + b_{f_1} \\ m_{89}\ \mathrm{PR}(89) + b_{89} \end{cases} \tag{4}$$

where variables m_{f_1} (m_{89}) and b_{f_1} (b_{89}) are slope and intercept, respectively, taking from Fig. 2 in potential GR(f_1/f_2) (PR(89)). As shown in Table II, excluding 2012, all differences were within ±3%, and all potential GR- and PR-based MPF retrievals tend to underestimate and overestimate, respectively, the original GR MPF retrieval. For GR(10/89)- and GR(18/89)-based MPF retrievals, the standard deviations were within few percent (∼3.8%). This is lower compared to the standard deviation (∼14.3%) of the GR(23/89), GR(36/89), and PR(89)-based MPF retrievals. These findings are also represented by the standard deviation of difference maps, shown in Fig. 3. These results suggest that the GR(10/89)-based MPF retrievals are available from AMSR-E/2 at a product quality most similar to the original GR(6/89)-based MPF retrieval.

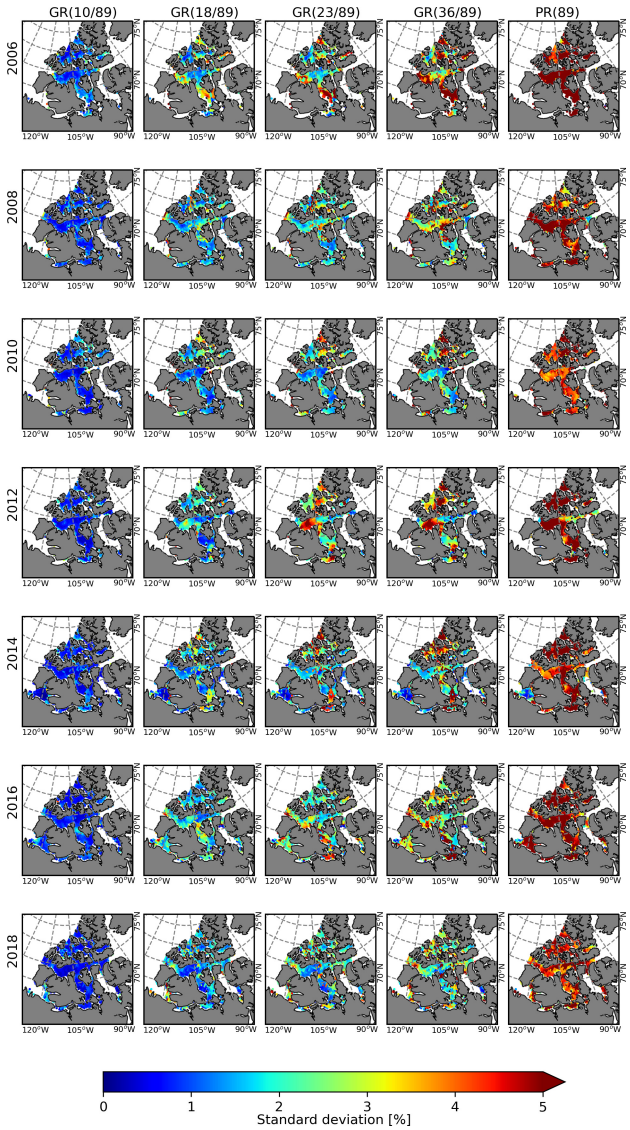

Fig. 3. Annual standard deviation maps of difference in MPFs retrieved from original GR(6/89) and potential GR(10/89), GR(18/89), GR(23/89), GR(36/89), and PR(89).

The original GR(6/89)-based MPF retrieval is valid for late melt season summer conditions, when bare ice and melt ponds

are prevalent [3] and available at a product quality similar to the MPF retrieved from optical remote sensing data when broadband albedo is around 0.5–0.7 [4]. It may, however, lead to an increase in pseudo-MPF estimates due to the decrease in H-pol T_B at 6 GHz that occurs when dry snow starts to melt [4]. Here we consider the period between MO and when melt ponds form on the ice (pond onset, PO) as a possible error since the snow is melting but there are no ponds yet. Generally, the PO in the CAA occurs 1–2 weeks after MO [12]. We attempted to constrain the analysis to the period after PO by doing the comparison shown in Fig. 2 for grid cells between MO + 2 weeks and FO. In all the combinations, the analysis with MO + 2 weeks only marginally improved the correlations (not shown). This is not unexpected since it is an intercomparison of MPFs retrieved from AMSR-E/2, and correlations between channels are expected even during the MO period before PO. An accurate determination of the PO could lead to better validation and application of the AMSR-E/2 MPF retrievals in the future.

Although even a snow wetness of a few percent strongly affects the microwave radiation, T_B in H-pol at 10.7 GHz is less influenced by wet snow variations, compared with around 6 and 37 GHz [6]. The GR(10/89)-based MPF retrieval may be useful for resolving the problem of snow wetness in the original MPF retrieval. However, the GR(10/89)-based MPF retrievals are still limited to MPF retrieval without land contamination due to the larger footprint of the order of ∼42 km at AMSR2 10.7 GHz.

Although the footprint size at 36.5 GHz (∼12 km for AMSR2) is smaller than that at 18.7 GHz (∼22 km for AMSR2), the higher frequency 36.5 GHz channel is more insensitive to liquid water than frequencies below 23.8 GHz [13]. Moreover, the footprints at 18.7 and 23.8 GHz are almost same. We therefore recommend that the MPF retrieval adopted for GR(18/89) is used in the narrow channel and nearshore environments like the CAA. When adopting GR(18/89) in (4), $m_{18} = 1.53$, $b_{18} = -0.0065$ for AMSR-E [Fig. 2(c)] and $m_{18} = 1.54$, $b_{18} = -0.0087$ for AMSR2 [Fig. 2(h)] are used. Although it is difficult to eliminate completely the land contamination at all frequencies, the contamination is much smaller at 18.7 GHz frequency than at 6.9 GHz.

Before AMSR-E, the understanding of long-term record of MPF is limited to the simulated evolution of melt ponds, e.g., [14]. In future work, the GR(18/89) might be ideal to use, along with the SSM/I-SSMIS T_B data including 19 GHz and around 90 GHz frequencies, for the understanding of longer-term record of MPF.

V. Conclusion

Based on an original GR(6/89)-based MPF retrieval, we examined the potential of an MPF retrieval method adopted to smaller footprint AMSR-E/2 channels, for situations where finer spatial resolution is advantageous such as the waterways of the CAA. For the potential retrieval, the same polarization (H-pol) was adopted as used in original MPF retrieval, but 10.7, 18.7, 23.8, 36.5, and 89.0 GHz frequencies were evaluated instead of 6.9 GHz frequency. Compared to the GR(6/89), the correlation and slope for GR(10/89) was highest and was close to 1, respectively. The correlations and slopes decreased and became steeper, respectively, in order of GR(10/89), GR(18/89), GR(23/89), GR(36/89), and PR(89). For GR(10/89)- and (18/89)-based MPF retrievals, the standard deviations were ∼3.8% over the evaluated period of 2006 to 2018. This is lower compared to the standard deviation (∼14.3%) of the GR(23/89)-, GR(36/89)-, and PR(89)-based MPF retrievals. Our results suggest that the GR(10/89)- and (18/89)-based MPF retrievals are available at a product quality similar to the original GR(6/89)-based MPF retrieval. We recommend that the MPF retrieval adopted GR(18/89) is used in narrow waterways such as in the CAA.

Acknowledgment

The AMSR-E and AMSR2 L1R brightness temperature swath products are available from the Japan Aerospace Exploration Agency (https://gportal.jaxa.jp/gpr/). The CIS charts in SIGRID-3 format and the daily SSM/I-SSMIS brightness temperature product were provided by the National Snow and Ice Data Center (NSIDC, https://nsidc.org/).

References

[1] S. Kern, A. Rösel, L. T. Pedersen, N. Ivanova, R. Saldo, and R. T. Tonboe, "The impact of melt ponds on summertime microwave brightness temperatures and sea-ice concentrations," *Cryosphere*, vol. 10, no. 5, pp. 2217–2239, Sep. 2016, doi: 10.5194/tc-10-2217-2016.

[2] S. Kern, T. Lavergne, D. Notz, L. T. Pedersen, and R. Tonboe, "Satellite passive microwave sea-ice concentration data set inter-comparison for arctic summer conditions," *Cryosphere*, vol. 14, no. 7, pp. 2469–2493, Jul. 2020, doi: 10.5194/tc-14-2469-2020.

[3] Y. Tanaka, K. Tateyama, T. Kameda, and J. K. Hutchings, "Estimation of melt pond fraction over high-concentration arctic sea ice using AMSR-E passive microwave data," *J. Geophys. Res., Oceans*, vol. 121, no. 9, pp. 7056–7072, Sep. 2016, doi: 10.1002/2016JC011876.

[4] Y. Tanaka, "Estimating meltwater drainage onset timing and duration of landfast ice in the canadian arctic archipelago using AMSR-E passive microwave data," *Remote Sens.*, vol. 12, no. 6, p. 1033, Mar. 2020, doi: 10.3390/rs12061033.

[5] G. Spreen, L. Kaleschke, and G. Heygster, "Sea ice remote sensing using AMSR-E 89-GHz channels," *J. Geophys. Res.*, vol. 113, no. C2, Jan. 2008, Art. no. C02S03, doi: 10.1029/2005JC003384.

[6] F. Ulaby and D. G. Long, *Microwave Radar and Radiometric Remote Sensing*. Annn Arbor, MI, USA: Univ. Michigan Press 2014.

[7] *Canadian Ice Service SIGRID-3 Implementation*, Canadian Ice Service (CIS), Environment, Toronto, ON, Canada, 2006.

[8] T. Maeda, Y. Taniguchi, and K. Imaoka, "GCOM-W1 AMSR2 level 1R product: Dataset of brightness temperature modified using the antenna pattern matching technique," *IEEE Trans. Geosci. Remote Sens.*, vol. 54, no. 2, pp. 770–782, Feb. 2016, doi: 10.1109/TGRS.2015.2465170.

[9] S. Marshall, K. A. Scott, and R. K. Scharien, "Passive microwave melt onset retrieval based on a variable threshold: Assessment in the canadian arctic archipelago," *Remote Sens.*, vol. 11, no. 11, p. 1304, May 2019, doi: 10.3390/rs11111304.

[10] T. Markus, J. C. Stroeve, and J. Miller, "Recent changes in arctic sea ice melt onset, freezeup, and melt season length," *J. Geophys. Res.*, vol. 114, no. C12, Dec. 2009, Art. no. C12024, doi: 10.1029/2009JC005436.

[11] W. N. Meier, H. Wilcox, M. A. Hardman, and J. S. Stewart, *DMSP SSM/I-SSMIS Daily Polar Gridded Brightness Temperatures, Version 5. [April-October From 2006 to 2018]*. Boulder, CO, USA: NASA National Snow and Ice Data Center Distributed Active Archive Center, Mar. 2020, doi: 10.5067/QU2UYQ6T0B3P

[12] S. E. L. Howell, A. Tivy, J. J. Yackel, and R. K. Scharien, "Application of a SeaWinds/QuikSCAT sea ice melt algorithm for assessing melt dynamics in the canadian arctic archipelago," *J. Geophys. Res.*, vol. 111, no. C7, 2006, Art. no. C07025, doi: 10.1029/2005JC003193.

[13] D. T. Eppler *et al.*, "Passive microwave signatures of sea ice," in *Microwave Remote Sensing of Sea Ice*, vol. 68, F. Carsey, Ed. Washington, DC, USA: AGU, Monograph, 1992, pp. 47–71.

[14] J. Zhang *et al.*, "Melt pond conditions on declining arctic sea ice over 1979–2016: Model development, validation, and results," *J. Geophys. Res., Oceans*, vol. 123, no. 11, pp. 7983–8003, Nov. 2018, doi: 10.1029/2018JC014298.